Available online at www.sciencedirect.com
SCIENCE DIRECT®
Separation and Purification Technology 42 (2005) 75–84
Separation and Purification Technology
www.elsevier.com/locate/seppur

Analysis and simulation of frontal affinity chromatography of proteins

Rosa Ma. Montesinos[a,1], Armando Tejeda-Mansir[b,*], Roberto Guzmán[c,2], Jaime Ortega[a,1], William E. Schiesser[d,3]

[a] *Departamento de Biotecnología y Bioingeniería, CINVESTAV-IPN. Avenida IPN No. 2508, México, D.F. 07360, México*
[b] *Departamento de Investigaciones Científicas y Tecnológicas. Universidad de Sonora, Apartado Postal 593, Hermosillo, Sonora, 83000, México*
[c] *Chemical and Environmental Engineering Department, University of Arizona, Tucson, AZ 85721, USA*
[d] *Iacocca D307111 Research Drive Lehigh University Bethlehem, PA 18015, USA*

Received in revised form 26 February 2004; accepted 2 March 2004

Abstract

A transport model that considers pore diffusion, external film resistance, finite kinetic rate and column dispersed flow, was used to mathematically describe a frontal affinity chromatography system. The corresponding differential equations system was solved in a simple and accurate form by using the numerical method of lines (MOL). The solution was compared with experimental data from literature and the analytic Thomas solution. The frontal affinity chromatography of lysozyme to Cibacron Blue Sepharose CL-6B was used as a model system. A good fit to the experimental data was made with the simulated runs of the transport model using the MOL solution. This approach was used to perform a parametric analysis of the experimental frontal affinity system. The influence of process and physical parameters on the frontal affinity chromatography process was investigated. The MOL solution of the transport model results in an unique and simple way to predict frontal affinity performance as well a better understanding of the fundamental mechanisms responsible for the separation.

Keywords: Frontal analysis; Mathematical modelling; MOL; Affinity chromatography; Proteins

1. Introduction

Affinity chromatography is now an industrial standard method used to economically purify high value proteins such as enzymes, monoclonal antibodies, hormones, vaccines, cytokines and clotting factors, present at very low concentrations in complex biological fluids such as liquid culture media and sera [1–4].

The conventional format for affinity separations is a packed column of porous adsorbent operating in frontal mode (also known as fixed-bed affinity adsorption). Four steps are involved in this operation mode: (1) adsorption, (2) washing, (3) elution and, (4) re-equilibration or regeneration. After the adsorption step, non-adsorbed material is washed off with the adsorption buffer, and then adsorbed solutes are eluted. Recovery is usually effected by changing the pH, ionic strength, or chemical composition of the buffer. To reuse the column a regeneration process must be conducted [5]. The key performance criteria for frontal affinity processes are breakthrough-curve sharpness and residence time at the adsorption stage.

The scale-up and optimization of affinity chromatographic operations is of major industrial importance [6–8]. The development of mathematical models to describe affinity chromatographic processes, and the use of these models in computer programs to predict column performance is an engineering approach that can help to successfully attain these bioprocess engineering tasks [9]. An important requirement of this methodology is a thorough understanding of the fundamental mechanisms underlying such separations in order to develop realistic models based on basic physical and chemical principles or rate theories. The equations obtained through this approach generally involve non-linear partial differential

* Corresponding author. Tel.: +52 662 259 21 69; fax: +52 662 259 21 97.
E-mail addresses: rosamamc@gauss.mat.uson.mx (R.M. Montesinos); atejeda@guayacan.uson.mx (A. Tejeda-Mansir); wes1@lehigh.edu (E. Schiesser).
[1] Tel.: +52 55 5061 3800.
[2] Tel.: +1 520 621 6041; fax: +1 520 621 6048.
[3] Tel.: +1 610 758 4264; fax: +1 610 758 5057.

1383-5866/$ – see front matter © 2004 Elsevier B.V. All rights reserved.
doi:10.1016/j.seppur.2004.03.014

Nomenclature

a	specific area/volume of the adsorbent particle (m^{-1})
c_0	initial protein concentration (mol/m^3)
c	protein concentration in the bulk liquid (mol/m^3)
c_i	protein concentration in the fluid of the pores (mol/m^3)
C	dimensionless protein concentration in the liquid
C_D	column diameter
d_p	adsorbent particle diameter (m)
D_{AB}	protein diffusivity in free liquid (m^2/s)
$D_E = \varepsilon_i D_i$	effective intraparticle protein diffusivity (m^2/s)
D_i	intraparticle protein diffusivity (free molecular diffusivity/pore tortuosity) (m^2/s)
D_L	column axial dispersion coefficient of the protein (m^2/s)
F	flow-rate (m^3/s)
k_1	adsorption rate constant ($m^3/(mol\,s)$)
k_2	desorption rate constant (s^{-1})
k_f	external film mass transfer coefficient (m/s)
K_d	equilibrium desorption constant, k_2/k_1
L	column length (m)
P	protein molecule
PS	protein-active site complex
q_i	protein concentration in the adsorbed phase of the adsorbent particles (mol/m^3)
q_m	maximum equilibrium concentration, mol/m^3 of solid volume of adsorbent
q_{ms}	maximum equilibrium concentration, mol/m^3 of settled volume of adsorbent
r	radial distance in the adsorbent particle (m)
r_m	radius of adsorbent particle (m)
R	dimensionless radius
S	active site
t	time (s)
T	dimensionless residence time in the column, $\upsilon t/L$
υ	interstitial column velocity (flow-rate/bed porosity-column area) (m/s)
X	dimensionless protein concentration in the liquid
z	axial distance in the column (m)
Z	dimensionless axial distance in the column

Greek letters

ε	bed porosity
ε_i	adsorbent particle porosity
μ	solution viscosity (g/m s)
ρ	solution density (g/m^3)
τ	dimensionless time, $D_E t/r_m^2$
ϕ	dimensionless protein concentration in the adsorbed phase
Υ	dimensionless separation factor
Γ	dimensionless effluent volume

equations (PDE) that are not amenable to analytical solutions. Computer programs need to be developed to solve these models.

Analytical solutions have been obtained through the rate-limited breakthrough approach which considered that only one rate limiting step, i.e. either rate of interaction or rate of diffusion (pore or film) is controlling the overall adsorption mechanism. The non-dispersive flow model is used in the analysis. Chase [10] used the Thomas solution, which involves Langmuir reaction kinetics as the rate-limiting step, to predict the performance of affinity separations. Hall et al. [11] have solved the non-dispersive model under the assumption of irreversibility, very fast reaction (equilibrium) and constant-pattern approach. These results were used by Arnold et al. [1] in the analysis of affinity separations. The applicability of these models is limited in the understanding and accurate prediction of the performance of the chromatographic process.

Hortsmann and Chase [12] used a two resistances model with an infinitely fast reaction and non-dispersed flow within the column, in modelling studies of the affinity adsorption of immunoglobulin G to protein A immobilized to agarose matrices. Numerical solution of the governing differential equations was carried out by a finite difference method using second order approximations in the space derivatives. The solution fitted well to the experimental data in almost all the experimental range. However, the method is impracticable for the solution of transport models that include dispersed flow and finite reaction rates.

Arve and Liapis [13] considered that the adsorption of a solute from the bulk solution on the surface of the adsorbent involves three discrete steps which contribute resistance to the mass transfer: film diffusion, pore diffusion and reaction kinetics. This approach along with a column dispersed-flow model was used by Berninger et al. [14] to present a generalized model to predict the performance of complex chromatography systems. The model was solved using the method of orthogonal collocation on finite elements.

Kempe et al. [6] used the three resistances model with column dispersed-flow for the simulation of affinity adsorption of lysozyme to Cibacron Blue Sepharose CL-6B. The mathematical model was solved applying the method of orthogonal collocation and an implicit numerical integrator based on Gear′s method. Very good overlap was obtained with the experimental data, except at the end of the breakthrough curve. This discrepancy increased as the experimental column length increased.

The method of orthogonal collocation requires more analytical work than the finite difference approach, and the analytical work is rather specific for the problem at hand. Furthermore, since the method generally uses linear polynomials it might be expected that a relatively large number of grid points has to be used to achieve accuracy in the PDE solution comparable to a higher order finite difference method.

There are two main strategies for the solution of adsorption PDEs: global methods and methods of lines. Both time and spatial derivatives are discretized in the so called global methods. The numerical method of lines (MOL) is a modular and flexible approach to programming partial differential equations solutions. The solution of the partial differential equations is performed in two steps: the boundary value derivatives are approximated by a discretization technique; then the remaining initial value problem is handled with an appropriate integrator. MOL has become the most widely used solution technique for large-scale time-dependent partial differential equations [15–18]. Although there are several software packages that use this methodology to solve two-dimensional problems, they are not usually easy to apply to adsorption equations, since adsorption is not described by truly two-dimensional models, but rather by two-region models [19].

In this work, a transport model that considers a dispersed flow in the column and three consecutive transport rate resistances to ideal equilibrium separation: external film resistance, particle internal diffusion and finite kinetic rate, is used for the simulation of the adsorption step of a frontal affinity chromatography process. Such models provide a general realistic description of almost all practical systems [20]. The work was oriented to show that an accurate solution of the transport model can be obtained using a simple numerical solution.

The solution of the model was obtained using the numerical method of lines. The solution was compared with experimental data from the literature of the adsorption of lysozyme to Cibacron Blue Sepharose CL-6B and the Thomas analytic solution of the lumped parameter column model [21]. The MOL solution of the transport model was used to perform a parametric analysis of the experimental system. The influence of process and physical parameters on the affinity process was investigated.

2. Frontal affinity chromatography model

During column operation in frontal mode the sample is fed continuously into the column. For a short time the solute in the feed is taken up almost completely, but after a while, solute breakthrough occurs and the effluent concentration increases with time. Much of the information needed to evaluate column performance is contained in these typical plots of effluent concentration versus time or breakthrough curves (BTC). These curves can be used to determine: (1) how much of the column capacity has been utilized, (2) how much solute is lost in the effluent, and (3) the processing time. This is precisely the performance information needed to optimize separation processing [1]. A mathematical model which can be used to accurately predict this dynamic behavior provides a practical way to obviate many experiments in the design and scale-up of a frontal affinity process.

2.1. Physical model

Many frontal affinity chromatography systems of industrial interest involve single-component adsorption. For this reason, in this study the frontal affinity model is based on the isothermal sorption of a single solute during flow through a porous fixed-bed of diffusive adsorbent particles with an average radius, r_m, and a porosity, ε_i, on which the ligand is immobilized. In this analysis, the feed protein concentration is, c_0, the protein solution in the system has a transient concentration, $c(z, t)$, with a constant interstitial flow-velocity, υ, through the column, with height, L, and a void-bed porosity, ε. The protein concentrations in the adsorbent fluid and solid phases are, c_i and q_i, respectively.

To achieve a mathematical description of a frontal affinity-chromatographic process, two major phenomena must be included: matrix hydrodynamics must be assessed, as well as the nature of the binding process itself. In this study, a transport model that considers a dispersed flow in the column and three consecutive transport rate resistances to ideal equilibrium separation is used for the simulation of the frontal affinity chromatography system.

The Fickian convective dispersion in the column is characterized by the axial dispersion coefficient, D_L. The transport of protein is considered to involve the interfacial transport of protein to the outer surface of the adsorbent particles from the bulk liquid through the adsorbent surrounding stagnant film characterized by the coefficient, k_f, the diffusion in the pore fluid described by an effective diffusion coefficient, D_E, and the adsorption step of the protein with active sites on the surface of the adsorbent. The intrinsic adsorption rate can be described by different kinetic models. In this study, an adsorption-desorption model of the Langmuir type is used.

2.2. Transport model

Due to the nonlinear equilibrium that characterizes affinity chromatography, adsorption behavior is best described by rate theories. This engineering approach to modelling involves the use of conservation equations, equilibrium laws at interfaces, kinetic laws of transport and adsorption and, initial and boundary conditions.

To describe the concentration change of protein with time at the column exit, the following equation can be derived by a solute mass balance in the fluid phase,

$$\frac{\partial c}{\partial t} - D_L \frac{\partial^2 c}{\partial z^2} + \upsilon \frac{\partial c}{\partial z} = -\frac{3}{r_m} \frac{(1-\varepsilon)}{\varepsilon} k_f (c - c_i)|_{r=r_m} \quad (1)$$

The equation to describe the change of concentration of solute in the fluid of the adsorbent pores can be obtained by a solute mass balance in the particle,

$$\varepsilon_i \frac{\partial c_i}{\partial t} + (1-\varepsilon_i)\frac{\partial q_i}{\partial t} = D_E\left(\frac{\partial^2 c_i}{\partial r^2} + \frac{2}{r}\frac{\partial c_i}{\partial r}\right) \quad (2)$$

To describe the complex interactions between solute and affinity adsorbent, simplified models are often used [1,10,12]. In general, a second-order reversible adsorption reaction is considered, where the solute is assumed to interact with the adsorbent by a monovalent interaction and characteristic constant binding energy:

$$P + S \rightleftharpoons PS$$

where P is the protein in solution, S is the ligand adsorption site and PS is the protein–ligand complex.

The rate of adsorption for this type of interaction is usually represented as

$$\frac{\partial q_i}{\partial t} = k_1 c_i (q_m - q_i) - k_2 q_i \quad (3)$$

where k_1 and k_2 are the adsorption and desorption rate constant, respectively. At equilibrium Eq. (3) gives the form of the Langmuir isotherm with equilibrium desorption constant $K_d = k_2/k_1$ and maximum adsorption capacity q_m.

At the beginning of the operation there is no protein present in the system, therefore

$$\text{at } t = 0, \quad c = 0, \quad 0 \le z \le L \quad (4)$$

$$\text{at } t = 0, \quad c_i = 0, \quad 0 \le r \le r_m \quad (5)$$

$$\text{at } t = 0, \quad q_i = 0, \quad 0 \le r \le r_m \quad (6)$$

The Danckwerts boundary conditions [22] are used to account for dispersion at the entrance of the column and complete mixing with only convection flow at the end of the column, and given by, respectively

$$\text{at } z = 0, \quad \varepsilon v c|_{z=0} - \varepsilon D_L \left.\frac{\partial c}{\partial z}\right|_{z=0} = \varepsilon v c_0, \quad t > 0 \quad (7)$$

$$\text{at } z = L, \quad \left.\frac{\partial c}{\partial z}\right|_{z=L} = 0, \quad t > 0 \quad (8)$$

Due to particle symmetry,

$$\text{at } r = 0, \quad \left.\frac{\partial c_i}{\partial r}\right|_{r=0} = 0, \quad t > 0 \quad (9)$$

At the mouth of the particle pore,

$$\text{at } r = r_m, \quad k_f (c - c_i)|_{r=r_m} = D_E \left.\frac{\partial c_i}{\partial r}\right|_{r=r_m}, \quad t > 0 \quad (10)$$

The frontal affinity model can be expressed in a dimensionless form using the following dimensionless variables:

$$C = \frac{c}{c_0}\ R = \frac{r}{r_m}\ T = \frac{vt}{L}\ \tau = \frac{D_E t}{r_m^2};\ \phi_i = \frac{q_i}{q_m};$$

$$Pe = \frac{vL}{D_L};\ Z = \frac{z}{L} \quad (11)$$

The corresponding dimensionless mass balance equations are:

$$\frac{\partial C}{\partial T} - \frac{1}{Pe}\frac{\partial^2 C}{\partial Z^2} + \frac{\partial C}{\partial Z} = -\frac{3}{r_m}\frac{(1-\varepsilon)L}{\varepsilon v} k_f\ (C - C_i)|_{R=1} \quad (12)$$

$$\frac{\partial C_i}{\partial \tau} + \frac{(1-\varepsilon_i) r_m^2 q_m k_1}{\varepsilon_i D_E c_0}\left[c_0 C_i (1-\phi_i) - K_d \phi_i\right] = \frac{1}{\varepsilon_i}\left(\frac{\partial^2 C_i}{\partial R^2} + \frac{2}{R}\frac{\partial C_i}{\partial R}\right) \quad (13)$$

the dimensionless adsorption rate,

$$\frac{\partial \phi_i}{\partial \tau} = \frac{r_m^2 k_1}{D_E}\left[c_0 C_i (1-\phi_i) - K_d \phi_i\right] \quad (14)$$

and the dimensionless initial and boundary conditions,

$$\text{at } T = 0, \quad C = 0, \quad 0 \le Z \le 1 \quad (15)$$

$$\text{at } T = 0, \quad C_i = 0, \quad 0 \le R \le 1 \quad (16)$$

$$\text{at } T = 0, \quad \phi_i = 0, \quad 0 \le R \le 1 \quad (17)$$

$$\text{at } Z = 0, \quad \left.\frac{\partial C}{\partial Z}\right|_{Z=0} = \frac{Lv}{D_L}\left(C|_{Z=0} - 1\right), \quad T > 0 \quad (18)$$

$$\text{at } Z = 1, \quad \left.\frac{\partial C}{\partial Z}\right|_{Z=1} = 0, \quad T > 0 \quad (19)$$

$$\text{at } R = 0, \quad \left.\frac{\partial C_i}{\partial R}\right|_{R=0} = 0, \quad T > 0 \quad (20)$$

$$\text{at } R = 1, \quad \left.\frac{\partial C_i}{\partial R}\right|_{R=1} = \frac{k_f r_m}{D_E}(C - C_i)|_{R=1}, \quad T > 0 \quad (21)$$

2.3. Numerical solution of the transport model

In this study, the model given by Eqs. (12)–(21) was solved using the numerical method of lines (Fig. 1). The DSS2D differential system simulator was used as the main program. It calls subroutines INITAL and PRINT to set and print the system initial conditions, respectively. Then subroutine INTEG is called to cover one print interval of the solution. INTEG in turn calls subroutine INT15 [which implements the Runge–Kutta Fehlberg 45 (RKF45) formulas] to compute the solution over the print interval. INT15 will, in general, call subroutine DERV many times during the calculation of the solution by numerical integration.

The system of ordinary differential equations which approximates the PDEs are programmed in subroutine DERV. This subroutine calls subroutine DSS034M to calculate the two-dimensional spatial derivatives $\partial C_i/\partial R$ and $\partial^2 C_i/\partial R^2$; DSS034M in turn calls the one-dimensional subroutines DSS004 and DSS044. To calculate the one-dimensional spatial derivatives $\partial C/\partial Z$ and $\partial^2 C/\partial Z^2$, DERV calls directly subroutines DSS004 and DSS044, which compute first and second derivatives, respectively, using five-point, fourth-order finite difference approximations [17].

To conduct the simulation studies, NR = 10 and NZ = 100 discretization points were used in the radial and axial dimensions, respectively. A grid analysis was used to compare the breakthrough curve sharpness using a different number of discretization points. Almost no effect was observed with an increase in the number of discretization points in the radial (NR = 20; NZ = 100) or in the axial (NR = 10 and NZ = 150) direction. These comparisons produced a mean square error of MSE = 1.63×10^{-9} and 4.38×10^{-6}, respectively. A significant increase in curve dispersion was observed with a decrease in the number of discretization points in the radial (NR = 5 and NZ = 100) or in the axial (NR = 10 and NZ = 50) direction. In these comparisons, the values of the mean square error where MSE = 6.30×10^{-5} and 0.179, respectively.

All the codes were incorporated in a Fortran 90 program that was run in a Compaq Alpha Server ES40 DEC660 with four CPU of 833 MHz. The computational time to obtain the complete breakthrough curve was 70 min.

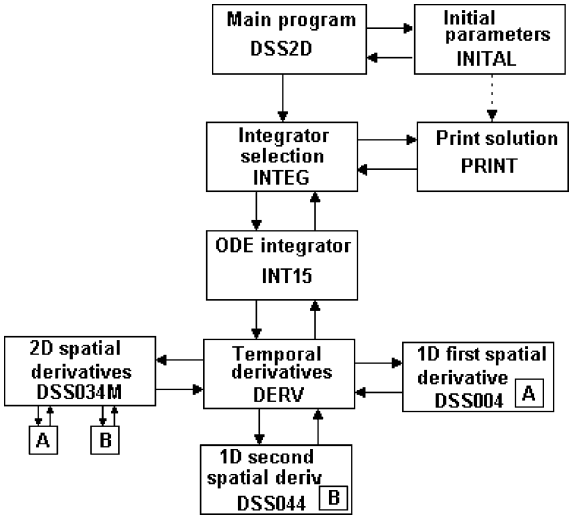

Fig. 1. Numerical method of lines solution scheme of the frontal affinity transport model.

2.4. Lumped parameter model

The most general relation that has been developed to describe breakthrough behavior involves Langmuir reaction kinetics as the rate-limiting step and non-dispersive convective flow through the column. It is known as the Thomas model [21]. Without mass-transfer effects on column performance, the overall rate of adsorption is only limited by the intrinsic adsorption kinetics. Another interpretation is that under mass-transfer limitations all effects of internal and external diffusion within and outside the beads as well as any dispersion in the column are lumped together with the kinetics. This approach is useful when mass-transfer resistance by pore-diffusion is relatively small. In this particular case, the analytical solution of the non-dispersive model is expressed as follows:

$$X = \frac{J\,(N/\Upsilon, N\Gamma)}{J(N/\Upsilon, N\Gamma) + \left[1 - J(N, N\Gamma/\Upsilon)\right] \exp\left[(1 - 1/\Upsilon)(N - N\Gamma)\right]} \tag{22}$$

where

$$X = \frac{c}{c_0} \tag{23}$$

$$\Gamma = \frac{\varepsilon K_\mathrm{d} \Upsilon (T-1)}{(1-\varepsilon) q_\mathrm{m}} \tag{24}$$

$$\Upsilon = 1 + \frac{c_0}{K_\mathrm{d}} \tag{25}$$

$$T = \frac{\upsilon t}{L} \tag{26}$$

$$N = \frac{(1-\varepsilon) q_\mathrm{m} k_1 L}{\varepsilon \upsilon} \tag{27}$$

and J is a two-parameter function of α and β, given by:

$$J(\alpha, \beta) = 1 - \mathrm{e}^{-\beta} \int_0^\alpha \mathrm{e}^{-\xi} I_o(2\sqrt{\beta\xi})\,\mathrm{d}\xi \tag{28}$$

where I_0 refers to the zero-order modified Bessel function of the first kind [23]. The analytical solution of Eqs. (22)–(28) (or Thomas model) was evaluated numerically for comparison with the numerical MOL solution and experimental data.

3. Input data for the study

The adsorption of lysozyme to Cibacron Blue Sepharose CL-6B was chosen as the model system. The values of the parameters utilized to conduct the simulation studies were obtained from the studies of Chase [10] and Kempe et al. [6] and are presented in Table 1.

To properly conduct this simulation, the experimental data were displaced one column residence time, because the time t in Chase's paper is measured from the time at which non-adsorbing species exit the column. In this work, t is measured

Table 1
Base case data used in simulation studies of frontal affinity adsorption of lysozyme to Cibacron Blue Sepharose CL-6B (Chase [10] and Kempe et al. [6])

Variable	Value
Inlet protein concentration	$c_0 = 7.14 \times 10^{-3}\,\mathrm{mol/m^3}$
Flow-rate	$F = 1.67 \times 10^{-8}\,\mathrm{m^3/s}$
Column length	$L = 0.014, 0.027, 0.041, 0.104\,\mathrm{m}$
Column diameter	$C_\mathrm{D} = 0.01\,\mathrm{m}$
Bed porosity	$\varepsilon = 0.39$
Bead porosity	$\varepsilon_i = 0.75$
Bead radius	$r_\mathrm{m} = 5 \times 10^{-5}\,\mathrm{m}$
Axial dispersion	$D_\mathrm{L} = 5.75 \times 10^{-8}\,\mathrm{m^2/s}$
Film mass-transfer rate	$k_\mathrm{f} = 6.9 \times 10^{-6}\,\mathrm{m/s}$
Solution viscosity	$\mu = 0.95\,\mathrm{g/m.s}$
Solution density	$\rho = 1.0 \times 10^{6}\,\mathrm{g/m^3}$
Lysozyme diffusivity in free liquid	$D_\mathrm{AB} = 1.06 \times 10^{-10}\,\mathrm{m^2/s}$
Effective diffusion coefficient	$D_\mathrm{E} = 5.3 \times 10^{-11}\,\mathrm{m^2/s}$
Adsorption rate constant (Transport model)	$k_1 = 1.144\,\mathrm{m^3/(mol\,s)}$
Adsorption rate constant (Thomas model)	$k_1 = 0.286\,\mathrm{m^3/(mol\,s)}$
Equilibrium desorption constant	$K_\mathrm{d} = 1.748 \times 10^{-3}\,\mathrm{mol/m^3}$
Maximum adsorption capacity	$q_\mathrm{ms} = 1.0\,\mathrm{mol/m^3}$
Maximum adsorption capacity of solid gel	$q_\mathrm{m} = 5.246\,\mathrm{mol/m^3}$

starting from the time at which the feed is introduced to the front of the bed. This last definition is commonly used in chromatography analysis because this time measurement is independent of the size of the non-adsorbing species, which is less ambiguous. The maximum adsorption capacity was calculated with respect to bed porosity, ε, and available volume to the protein as $q_\mathrm{m} = 0.8 \times q_\mathrm{ms}/[(1-\varepsilon)(1-\varepsilon_i)]$.

In the analysis of the influence of bead diameter on the affinity process the mass-transfer coefficient was estimated using the Foo and Rice correlation [24],

$$Sh = 2 + 1.45\, Re_\mathrm{p}^{1/2} Sc^{1/3} \tag{29}$$

where

$$Sh = \frac{k_\mathrm{f} d_\mathrm{p}}{D_\mathrm{AB}}, \quad Sc = \frac{\mu}{\rho D_\mathrm{AB}}, \quad Re_\mathrm{p} = \frac{d_\mathrm{p}\,(\varepsilon\upsilon)\,\rho}{\mu} \tag{30}$$

Also, as stated by Kempe et al. [6] the value of the Peclet number was set to 1 and the axial dispersion coefficient was calculated with the following expression:

$$Pe = \frac{\upsilon d_\mathrm{p}}{D_\mathrm{L}} \tag{31}$$

4. Results and discussion

The solution to the transport model for frontal affinity chromatography of lysozyme to Cibacron Blue Sepharose CL-6B was obtained using the MOL. This solution was compared with the experimental data and with the analytical solution of the lumped parameter model. Four column lengths were considered: 0.014, 0.027, 0.041 and 0.104 m. The results are shown in Fig. 2.

Taking into account the four column lengths, the average of the residual sum of squares between model calculations and experimental data were 0.0192 ± 0.0089 and 0.1185 ± 0.0051 for the MOL and the Thomas solution, respectively. A much better fit to the experimental data was obtained using MOL solution with the base parameter values. In these computations, the kinetic parameter value was set to $k_1 = 1.144\,\mathrm{m^3/mol\,s}$, since in the transport model this is not a lumped parameter. The simulation runs with the Thomas model using the value for the lumped parameter $k_1 = 0.286\,\mathrm{m^3/mol\,s}$ fitted fairly well to the experimental data.

In order to study how the transport model solution is able to account for variations in operating characteristics with system parameters, a parametric analysis was performed by overlaying frontal affinity curves from several computer

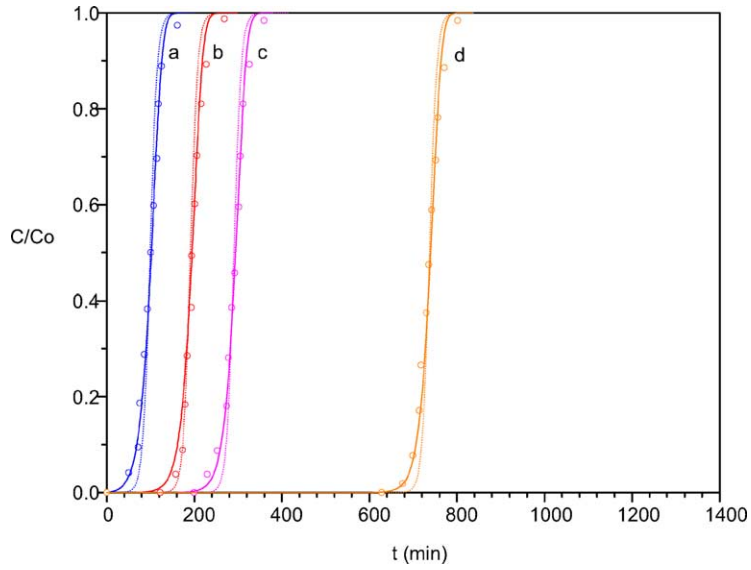

Fig. 2. Transport and lumped kinetic parameter models compared with frontal affinity chromatography experimental data (Chase [10]). Operating conditions according to Table 1. (○) Experimental data. (—) Numerical method of lines solution of the transport model. (· · ·) Lumped parameter model. The column lengths used were (a) 0.014 m (b) 0.027 m, (c) 0.041 m and (d) 0.104 m.

simulations, in which one parameter was changed while the others were kept constant at the basic set of values in Table 1 and using a column length of $L = 0.014$ m. The effect of inlet protein concentration and bead diameter is reported.

Upstream perturbations can initiate changes in process inlet concentrations that are important for study. The inlet protein concentration was changed using ±20 and ±40% variations of the $c_0 = 7.14 \times 10^{-3}$ mol/m^3 base value. The corresponding curves are shown in Fig. 3. An increased inlet concentration gives an early and sharper breakthrough curve. As the inlet concentration increases, the driving-force for the transport process is also augmented. This results in a faster saturation of the adsorbent beads. When the beads became saturated more rapidly, they will extract protein from the mobile phase for a shorter time, resulting in a sharper breakthrough curve. Hence, on this basis, it is more efficient to apply solute at high concentration. The utilization of the maximum capacity of the bed is greater at higher solute concentration as these conditions favor a greater extent of adsorption at equilibrium. As reported by Chase [10], when the dimensionless exit concentration of the column is plotted against the adsorbent applied to the column, an effect is only

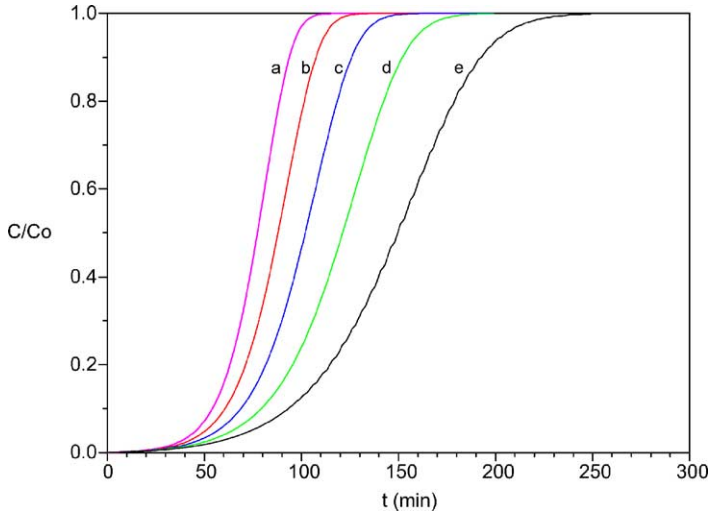

Fig. 3. Influence of the inlet protein concentration to the column on the affinity breakthrough behavior. Operating conditions according to Table 1 with the column length of $L = 0.014$ m: (a) +40%, (b) +20%, (c) $c_0 = 7.14 \times 10^{-3}$ mol/m^3, (d) −20 and (e) −40%.

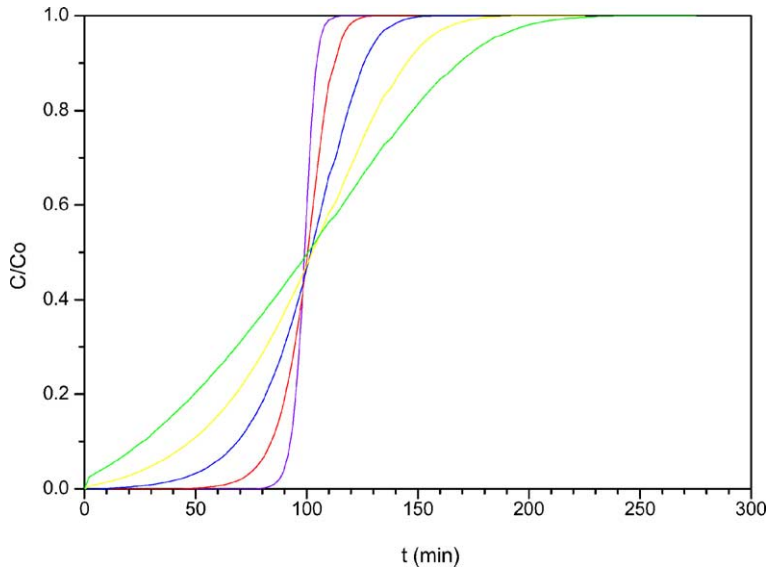

Fig. 4. Influence of the bead diameter on affinity breakthrough behavior. Operating conditions according to Table 1 with the column length of $L = 0.014$ m: (a) −80%, (b) −40%, (c) $d_p = 100$ μm, (d) +40% and, (e) +80%.

noticed on the shape and position of the breakthrough curve when the inlet concentration, c_0, is comparable or smaller than the desorption equilibrium constant, K_d. The shape and position of the breakthrough curve becomes constant when $c_0 >> K_d$.

The process parameter of most interest is the bead diameter. The bead diameter was changed using ±40 and ±80% variations of the $d_p = 100$ μm base value. The corresponding curves are shown in Fig. 4. A sharper breakthrough curve and consequently a greater operation capacity is obtained as the bead diameter decreases. It can also be noted from the figure that this effect is less dramatic as the bead size decreases. As particle diameter decreases the initial adsorption rate increases markedly, since the diffusion time is decreased due to the shorter diffusion path. At the same time the area/volume ratio for a single particle $(3/r_m)$ increases, giving an increased

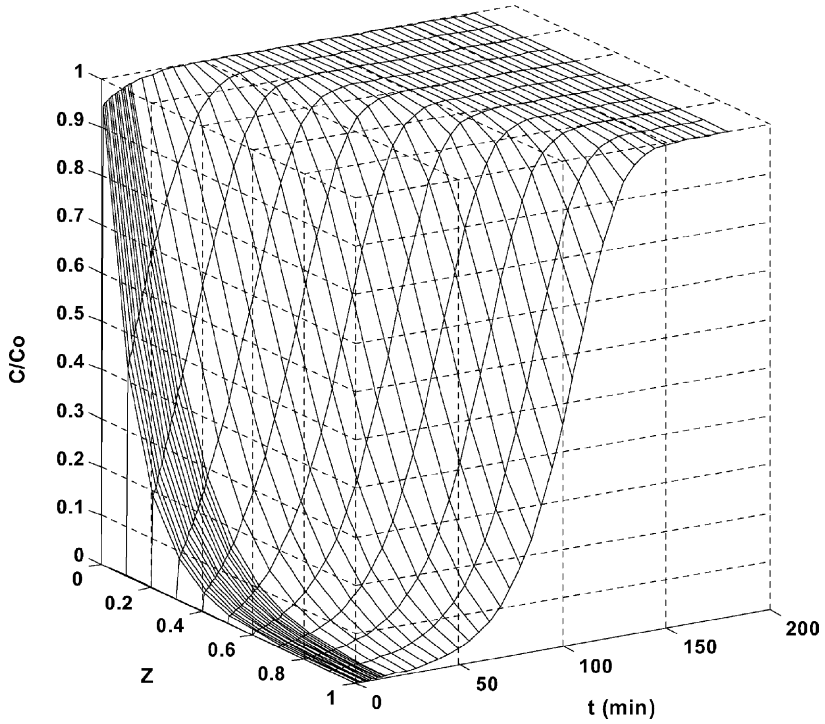

Fig. 5. Variation of the dimensionless protein concentration in the bulk liquid, c/c_0, with the dimensionless column length, Z, and the real time, t.

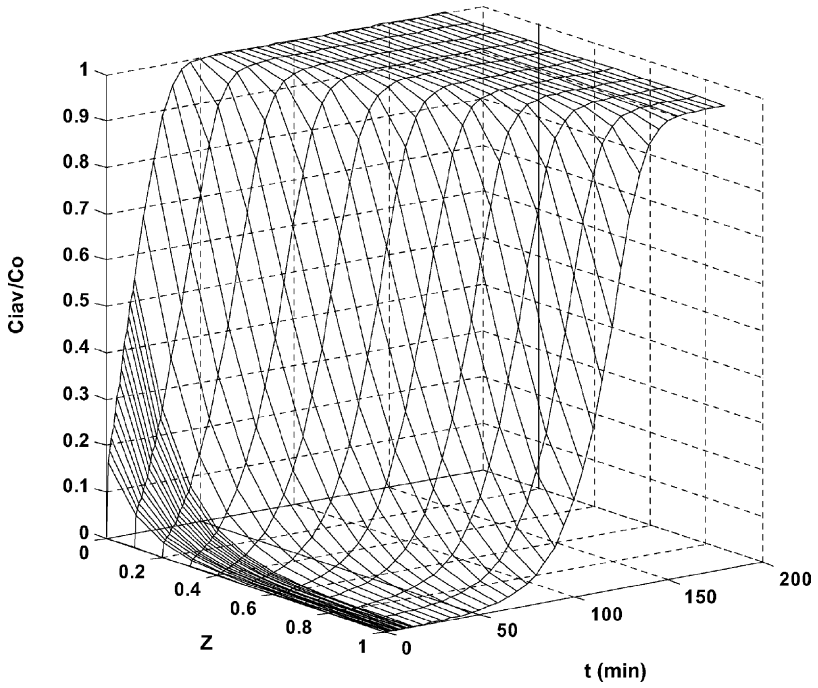

Fig. 6. Variation of the average dimensionless protein concentration in the adsorbent pore liquid, c_i/c_0, with the dimensionless column length, Z, and the real time, t.

mass transfer area between the surrounding liquid phase and the bead. Both factors contribute to the increase in total adsorption rate.

The MOL solution of the transport model was also used to describe in more detailed form the affinity chromatography process, e.g. detailing the protein dimensionless concentration profiles in the bulk liquid at the column end, c/c_0; in the adsorbent pore liquid (average), c_i/c_0; and in the adsorbed phase (average), q_i/q_m; as function of the dimensionless column length, Z, and the real time, t, (Figs. 5–7). The concentration profiles in Fig. 5 are very symmetric suggesting the importance of both liquid film and pore diffusion mass transfer resistances in the adsorption process. The total column equilibration occurs in about 150 min. The high slope of the

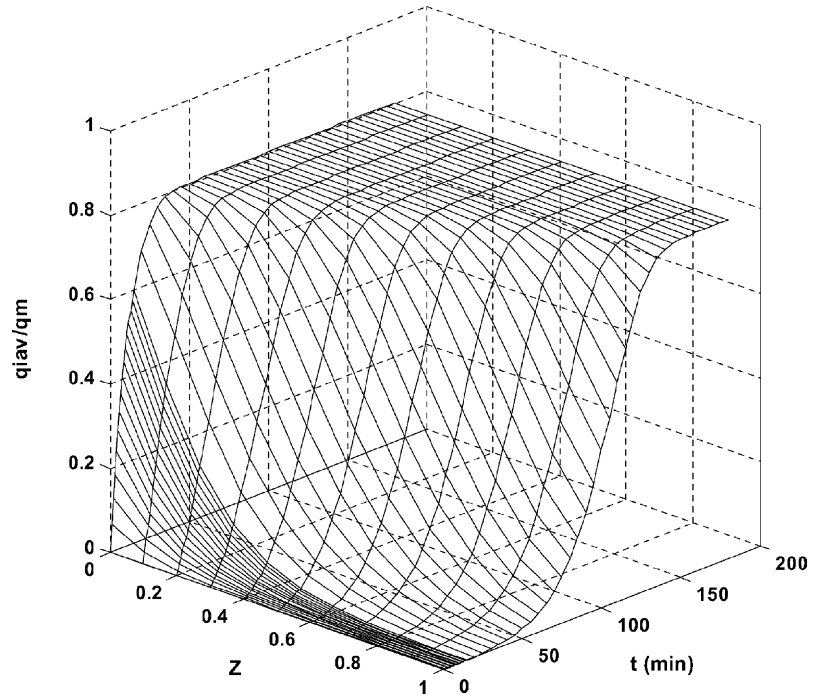

Fig. 7. Variation of the average dimensionless protein concentration in the adsorbed phase, q_i/q_m, with the dimensionless column length, Z, and the real time, t.

curves in the 0.5 region indicates the additional contribution of the dispersion to curve spreading. The film mass transfer resistance and dispersion effect can also be observed in Fig. 6. At the column entrance, the average protein concentration in the adsorbent pore liquid reached the column inlet concentration in about 40 min. Consequently, when comparing the Figs. 5 and 6 profiles, an obvious positive concentration gradient is always present along the adsorption process except at the end when breakthrough occurs. The protein concentration profile in the adsorbed phase shown in Fig. 7, reach a maximum value of 0.8 which is the concentration in the adsorbent in equilibrium with the column inlet protein concentration, in accordance with a Langmuir isotherm. Analogously, when comparing the Figs. 6 and 7 profiles, a positive concentration gradient is also present.

5. Conclusions

The performance of frontal affinity chromatography of lysozyme to Cibacron Blue Sepharose CL-6B Sepharose was successfully described with a three-resistances and column dispersed flow model. Programming the model solution was relatively simple using MOL. The parametric analysis conducted helps to show the influence of both operation and system parameters on the affinity process. An early and sharper breakthrough curve and therefore a greater operating throughput of the affinity process is obtained with increased column inlet concentrations. In the bead-size parametric study, a sharper breakthrough curve and consequently a greater operating throughput was obtained as the bead diameter decreases. This effect was less dramatic as the bead size decreases. The dynamic responses obtained are in concordance with theoretical predictions and show that the transport model can be used as a framework to provide a general description of almost all practical systems, when the appropriate basic experimental parameters and numerical solution are used. The MOL solution of the transport model permitted an accurate prediction of the frontal affinity performance and a better understanding of the fundamental mechanisms responsible for the separation. The influence of the adsorption properties of the protein from other components present in more complex mixtures, should enable the work described here with a model system to be extended to more practical situations. We plan a similar analysis for multicomponent systems.

Acknowledgments

The authors gratefully acknowledge the support of this work by the Consejo Nacional de Ciencia y Tecnología de México under grant No. U39963Z and by the Programa de Mejoramiento del Profesorado de la Secretaría de Educación Pública de México through the grant EXB-01-01 PROMEP-SEP.

References

[1] F.H. Arnold, H.W. Blanch, C.R. Wilke, Chem. Engng. J. 30 (1985) 9.
[2] Y.D. Clonis, J.A. Asenjo (Eds.), Separation Processes in Biotechnology, Marcel Dekker, New York, 1990, p. 801.
[3] F.M. Steinberg, J. Raso, Biotech Pharmaceuticals and Biotherapy, American Council on Science and Health, New York, 1998, p. 31.
[4] A.I. Liapis, Sep. Purif. Meth. 19 (1990) 133.
[5] A.I. Liapis, J. Biotechnol. 11 (1989) 143.
[6] H. Kempe, A. Axelsson, B. Nilsson, G. Zacchi, J. Chromatogr. A 846 (1999) 1.
[7] R.L. Fahrner, H.V. Iyer, G.S. Blank, Bioprocess. Eng. 21 (1999) 287.
[8] A. Tejeda, J.A. Noriega, J. Ortega, R. Guzmán, Biotechnol. Prog. 14 (1998) 493.
[9] A.I. Liapis, K.K. Unger, G. Steet (Eds.), Highly Selective Separations in Biotechnology, Chapman and Hall, Glasgow, NZ, 1994, p. 121.
[10] H.A. Chase, J. Chromatogr. 297 (1984) 179.
[11] K.R. Hall, L.C. Eagleton, A. Acrivos, T. Vermeulen, Ind. Eng. Chem. Fundam. 5 (1966) 212.
[12] B.J. Horstmann, H.A. Chase, Chem. Eng. Res. Des. 67 (1989) 243.
[13] B.H. Arve, A.I. Liapis, AIChE J. 33 (1987) 179–193.
[14] J.A. Berninger, R.D. Whitley, X. Zhang, N.H.L. Wang, Comput. Chem. Eng. 15 (1991) 749.
[15] W.E. Schiesser, The Numerical Method of Lines: Integration of Partial Differential Equations, Academic Press, San Diego, CA, 1991, p. 326.
[16] W.A. Vande, P. Saucez, W.E. Schiesser, Adaptive Method of Lines, CRC Press, Boca Raton, FL, 2001, p. 432.
[17] C.A. Silebi, W.E. Schiesser, Dynamic Modeling of Transport Process Systems, Academic Press Inc., San Diego, CA, 1992, p. 518.
[18] W.E. Schiesser, C.A. Silebi, Computational Transport Phenomena: Numerical Methods for the Solution of Transport Problems, Cambridge University Press, Cambridge, UK, 1997, p. 457.
[19] C. Costa, A. Rodrigues, A. Rodrigues (Eds.), Adsorption: Science and Technology, Kluwer Academic Publishers, The Netherlands, 1986, p. 257.
[20] D.M. Ruthven, Principles of Adsorption and Adsorption Processes, John Wiley & Sons, New York, 1984, p. 220.
[21] H.C. Thomas, J. Am. Chem. Soc. 66 (1944) 1664.
[22] P.V. Danckwerts, Chem. Eng. Sci. 2 (1953) 219.
[23] N.K. Hiester, T. Vermeulen, Chem. Eng. Prog. 48 (1952) 505.
[24] S.C. Foo, R.G. Rice, AIChE J. 21 (1975) 1149.